LETTER

doi:10.1038/nature12371

An observed correlation between plume activity and tidal stresses on Enceladus

M. M. Hedman[1], C. M. Gosmeyer[2], P. D. Nicholson[1], C. Sotin[3], R. H. Brown[4], R. N. Clark[5], K. H. Baines[3], B. J. Buratti[3] & M. R. Showalter[6]

Saturn's moon Enceladus emits a plume of water vapour and micrometre-sized ice particles from a series of warm fissures located near its south pole[1–10]. This geological activity could be powered or controlled by variations in the tidal stresses experienced by Enceladus as it moves around its slightly eccentric orbit. The specific mechanisms by which these varying stresses are converted into heat, however, are still being debated[11–16]. Furthermore, it has proved difficult to find a clear correlation between the predicted tidal forces and measured temporal variations in the plume's gas content[17–19] or the particle flux from individual sources[20,21]. Here we report that the plume's horizontally integrated brightness is several times greater when Enceladus is near the point in its eccentric orbit where it is furthest from Saturn (apocentre) than it is when near the point of closest approach to the planet (pericentre). More material therefore seems to be escaping from beneath Enceladus' surface at times when geophysical models predict its fissures should be under tension[12,15,16] and therefore may be wider open.

This analysis focuses on 252 images of the Enceladus plume at wavelengths of 0.88–1.56 μm obtained by the Cassini spacecraft's Visual and Infrared Mapping Spectrometer (VIMS)[22] between 2005 and 2012 (see Supplementary Information). Although these VIMS observations could not resolve individual jets and sources, they all had sufficient resolution and signal-to-noise ratio to detect the plume as a whole (see Fig. 1). The position of Enceladus along its orbit during each of these observations is given by the 'orbital phase', f: that is, the difference between the moon's orbital longitude and the longitude of its pericentre (also known as the moon's true anomaly). For the data considered here, f varies between -40° and $+200^\circ$. Hence the observations sample times when Enceladus was near the pericentre ($f \approx 0^\circ$) and near the apocentre ($f \approx 180^\circ$) of its eccentric orbit, and span a broad range of tidal stress states.

Measurements made at different orbital phases and different times can only be sensibly compared to one another if we also account for variations in the viewing geometry, especially the phase angle α (that is, the angle between the light rays incident on the plume and the scattered light rays that reach the camera). The micrometre-sized plume particles are most efficient at scattering light at large phase angles[6], so the plume will appear brighter when viewed at higher phase angles. Fortunately, the VIMS observations covered a range of phase angles when Enceladus was near the pericentre and the apocentre of its eccentric orbit, so we can control and compensate for these brightness variations due to changes in the viewing geometry. For example, the data shown in Fig. 1 compare measurements made at two different orbital phases for two different phase angles. At both phase angles the plume is brighter in the observation obtained when Enceladus was near the apocentre of its orbit, which strongly suggests that tidal forces do play an important role in controlling Enceladus' activity.

Owing to variations in the distance between Cassini and Enceladus, different observations sample the plume's brightness at different altitudes. Hence, in order to derive comparable quantitative estimates of the plume's brightness, we interpolate the brightness data from each observation to a common altitude. Fortunately, the plume's brightness decreases with altitude in a regular manner. Let us define the plume's 'equivalent width' (EW) at a given altitude z above Enceladus' south pole as the total integrated brightness in a horizontal slice through the plume (that is, a fixed z) after removing any background signal from Saturn's E ring (see Supplementary Information). For low-optical-depth systems like the plume, this quantity is insensitive to both the image resolution and the alignment of the fissures, which facilitates comparisons between different observations. Furthermore, as shown in Fig. 2, EW is a nearly linear function of the parameter Z ($= [z/(r_E + z)]^{1/2}$, where $r_E = 250$ km is the radius of Enceladus). This trend is not only a useful empirical fit to the data, it can also be physically justified on the basis of considerations of the velocity distribution of the plume particles[7]. For the observable parts of the plume, we can assume that the particle and gas density are so low that the particles follow purely ballistic trajectories and that Enceladus' gravity is by far the dominant force acting on the particles. In this situation, an individual particle launched from the surface at a velocity v_o that is less than Enceladus' escape speed, $v_{esc} = 240\ \mathrm{m\ s^{-1}}$, will reach an altitude z_{max} before it falls back to the surface. The velocity of the particle passes through zero when it reaches z_{max}, and energy conservation requires that $v_o = v_{esc}[z_{max}/(r_E + z_{max})]^{1/2}$. Hence a particle launched at speed v_o spends the most time near $Z = v_o/v_{esc}$ and makes the largest contribution to the plume's brightness at that location. Hence the steady decrease in the plume's brightness as a function of Z implies that fewer particles are launched at higher velocities, consistent with previous analyses[7].

Fitting the plume's EW profile in each image to a linear function of Z for altitudes between 50 and 450 km (that is, Z between 0.4 and 0.8), we may estimate EW_{85}, the plume's equivalent width at an altitude of 85 km (that is, $Z = 0.5$) for each observation. Figure 3 plots these estimates of the plume's brightness as a function of the observed phase angle. Note that at any given phase angle, observations taken when Enceladus was near its orbital apocentre are systematically brighter than those taken when Enceladus was near its orbital pericentre. (This trend persists even if we control for other geometric parameters like the sub-spacecraft latitude or longitude.) Furthermore, the data obtained when Enceladus was close to either its pericentre or its apocentre appear to follow a simple empirical phase function $P(\alpha)$ where the brightness is a power-law function of the scattering angle $\theta = 180^\circ - \alpha$ with an index of around 2.5 (that is, $P(\alpha) \propto \theta^{-2.5}$, see Fig. 3). We may therefore define a 'corrected equivalent width', $CEW = EW_{85} \times [\theta/20^\circ]^{+2.5}$. So long as the plume's phase function is approximately proportional to $\theta^{-2.5}$, then these corrected widths should be nearly independent of phase angle and

[1]Center for Radiophysics and Space Research, Cornell University, Ithaca, New York 14853, USA. [2]Department of Astronomy, Indiana University, Bloomington, Indiana 47405, USA. [3]Jet Propulsion Laboratory, California Institute of Technology, 4800 Oak Grove Drive, Pasadena, California 91109, USA. [4]Department of Planetary Sciences, Lunar and Planetary Laboratory, University of Arizona, Tucson, Arizona 85721, USA. [5]United States Geological Survey Mail Stop 964, Box 25046, Denver Federal Center, Denver, Colorado 80225, USA. [6]SETI Institute, 189 Bernardo Avenue Suite 100, Mountain View, California 94043, USA.

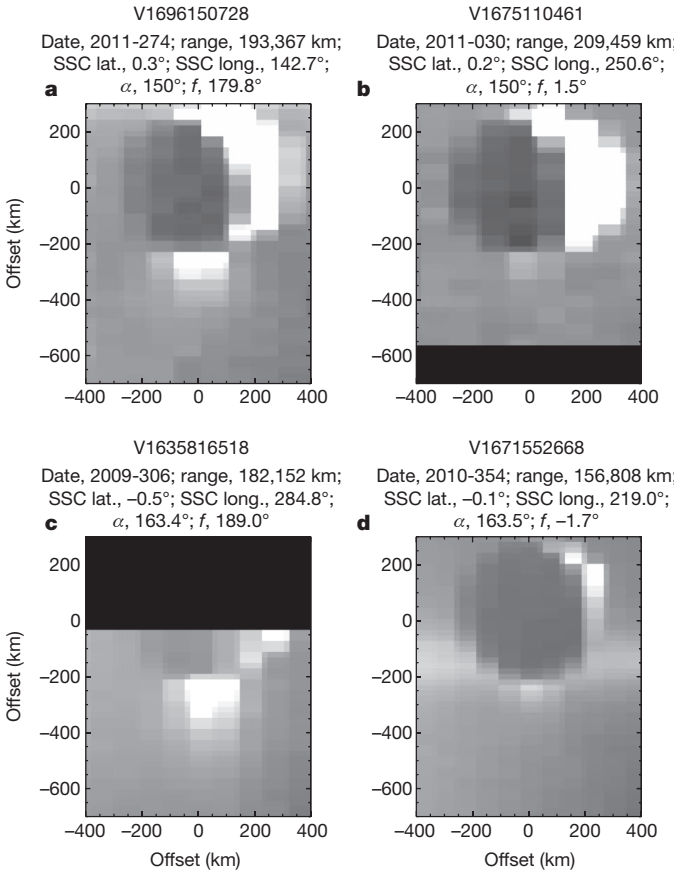

Figure 1 | Sample VIMS observations of Enceladus and its plume. All the images are made at wavelengths of 0.88–1.56 μm, have been rotated so that Enceladus' north pole points straight up, and have been projected onto a common spatial scale. In each panel, Enceladus appears as a dark disk silhouetted against the E-ring. The bright crescents at the upper right of these disks correspond to the illuminated part of the moon, and the plume appears as a diffuse bright streak below the moon's south pole (compare with Supplementary Fig. 2). Black regions correspond to regions not covered by the original observation. The observation name is given at the top of each panel, with the relevant observation date and geometric parameters (see Supplementary Information). Images **a** and **b** were obtained at a phase angle (α) of 150°, whereas images **c** and **d** were acquired at $\alpha \approx 163.5°$. Images taken at the same phase angle use the same stretch, but the images taken at a phase angle of 150° have a different stretch from the ones obtained at around 163.5° phase. Note that the plume is significantly brighter in **a** and **c** (where Enceladus was near its orbital apocentre), than it is in **b** and **d** (where the moon was near its orbital pericentre). Above each panel are given: date (year-day); range (distance between the spacecraft and Enceladus), sub-spacecraft latitude (SSC lat.); sub-spacecraft longitude (SSC long.); phase angle α; and orbital phase, f.

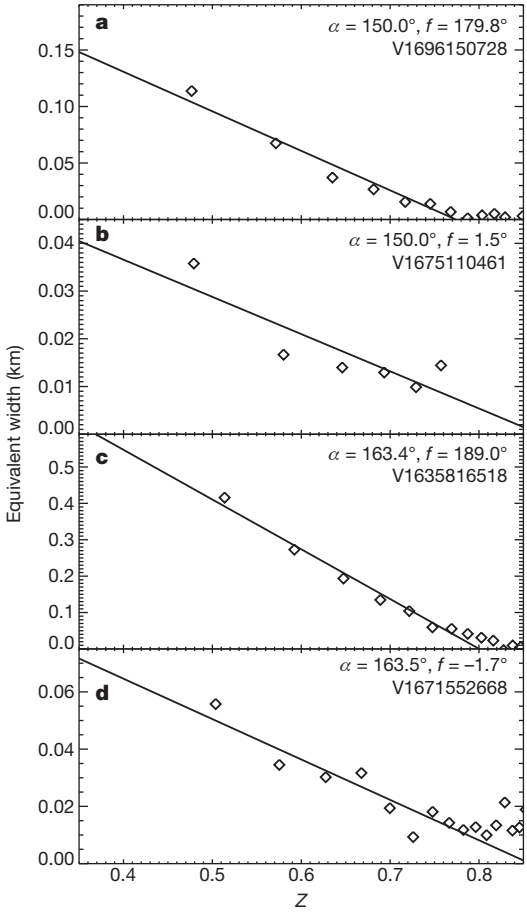

Figure 2 | Sample vertical profiles of the plume's brightness. a–d, The plume's equivalent width as a function of $Z = [z/(r_E + z)]^{1/2}$ for the four observations shown in Fig. 1a–d respectively. (As discussed in the text, Z can be regarded as a proxy for the particles' launch velocity.) In each panel, the diamonds show the measurements while the line shows a simple linear fit to the data between altitudes z of 50 and 450 km ($Z = 0.4$ and 0.8, respectively). This range was chosen because it excludes regions that are either too close to Enceladus (where the moon's limb may contaminate the signal) or too far from the moon (where the signal is weak). Note that in all four cases, this simple model provides a reasonable match to the trends in the data.

correspond to the plume brightnesses VIMS would have measured if it had always observed the plume at a phase angle of 160°.

Figure 4 shows a plot of the resulting corrected equivalent width estimates as a function of Enceladus' orbital phase. Note that the data from different phase angles follow the same trend, indicating that our approximate phase function is reasonably successful at correcting all these data. This plot confirms that the plume is indeed substantially brighter when Enceladus is at apocentre than when it is at pericentre. In fact, the plume's integrated brightness increases by more than a factor of three as Enceladus moves from pericentre to apocentre, and most of this change seems to occur between orbital phases of 90° and 180°.

Initial investigations of the longer-wavelength data obtained by VIMS reveal the same basic trends with orbital phase, albeit at lower signal-to-noise ratio. Thus far we have not detected any statistically significant variations in the shape of the plume's spectrum between observations taken when Enceladus is at pericentre versus apocentre, implying that the observable particle size distribution is not a strong function of orbital phase.

Similarly, the data taken between 2009 and 2012 all exhibit the same variations with orbital phase (see Fig. 4), indicating that the plume's activity level at a given orbital phase has not changed radically in the past few years. However, the 2005 observations yield brightness levels that are roughly 50% higher than comparable later observations. This may represent a decrease in the plume's average activity level between 2005 and 2009. However, even if this turns out to be the case, the 2005 data show the same trend of increasing brightness with increasing orbital phase as the later data. The variation in the plume's activity on orbital timescales therefore appears to be a persistent phenomenon.

These trends are also insensitive to altitude up to 300 km from the moon's surface (where the plume is clearly detectable). However, at higher altitudes, these trends might reverse owing to variations in the plume's scale height with orbital phase. In Fig. 2, the linear fits for the two observations made when Enceladus was close to its orbital apocentre intercept the x-axis when $Z \approx 0.8$. By contrast, the two observations made when Enceladus was near its orbital pericentre yield trends that go to zero when Z is at least 0.85. This distinction appears to be found consistently among the other observations: the weighted average of the x-intercepts for the profiles obtained when Enceladus was within ±40° of pericentre occurs at $Z = 0.835 \pm 0.013$, whereas for the

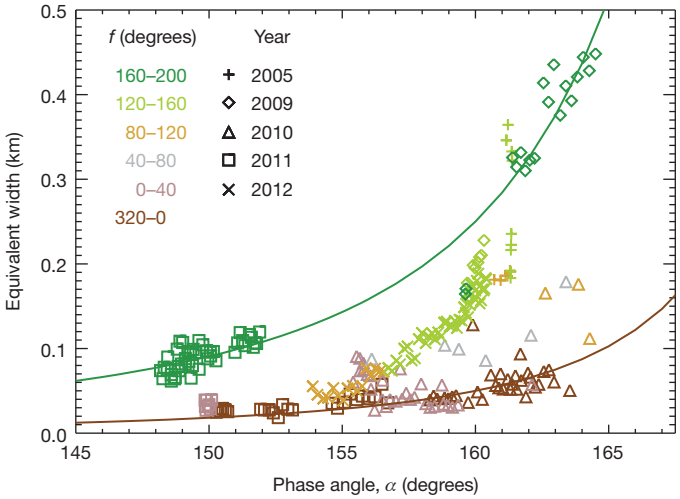

Figure 3 | Variations in the plume's brightness with phase angle. This plot shows the plume's equivalent width at 85 km altitude ($Z = 0.5$) and 0.88–1.56 μm as a function of phase angle α. Colours indicate observations made when Enceladus was at different orbital phases f, and symbols indicate when the observations were taken. The 1 s.d. statistical error bars on these data points are smaller than the symbol sizes (they range between 0.001 and 0.03, with most being between 0.005 and 0.01, see Supplementary Information). This plot shows that at all phase angles, the plume is consistently brighter when it is observed close to Enceladus' orbital apocentre. The two lines show fiducial phase functions that are proportional to $\theta^{-2.5}$, where θ is the scattering angle. The data obtained near Enceladus' apocentre follow this phase function fairly closely. For the pericentre data, the data do not match the predicted trend quite as well, but the above phase function is still an acceptable approximation to the true phase curve.

data obtained within ±20° of apocentre the average intercept occurs at $Z = 0.793 \pm 0.008$. This can be interpreted as a difference in the maximum launch velocity of the observed particles, with $v_{max} = 200 \pm 3$ m s^{-1} when Enceladus is near pericentre and $v_{max} = 190 \pm 2$ m s^{-1} when Enceladus is near apocentre. Hence the particles visible at 0.88–1.56 μm seem to be launched with a slightly larger maximum speed

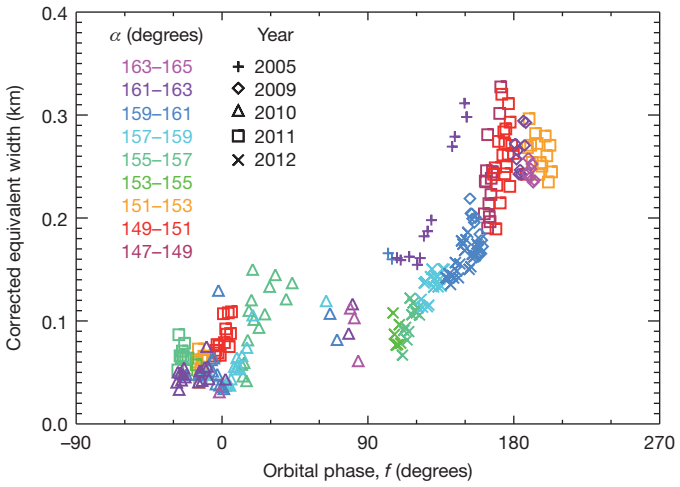

Figure 4 | Variations in the plume's corrected brightness with Enceladus' orbital position. This plot shows the plume's corrected equivalent width at 85 km altitude and 0.88–1.56 μm as a function of Enceladus' orbital phase f. Colours indicate observations made at different phase angles α, and symbols indicate when the observations were taken. The 1 s.d. statistical error bars on these data are smaller than the symbol sizes (they range between 0.001 and 0.03, with most being between 0.005 and 0.015, see Supplementary Information). Note that these data have now been corrected to remove the brightness variations due to varying phase angles by multiplying all the EW_{85} values by a factor of $(\theta/20°)^{2.5}$. With this correction applied, the data taken at different phase angles follow a common trend with orbital phase.

when Enceladus is near its orbital pericentre. This could reflect tidally induced changes in the crack geometry[23]. However, this trend is much more subtle than the variation in brightness, and so additional work will be needed before we can securely interpret this phenomenon.

A peak in plume activity when Enceladus is near its orbital apocentre is consistent with various geophysical calculations that suggest the normal stresses in Enceladus' south polar terrain will place the fissures under tension when Enceladus is near apocentre, and in compression when Enceladus is near pericentre[11,12,15,16,21]. Hence the data we report here provide strong evidence that tidal forces do play an important role in controlling Enceladus' plume activity, perhaps by changing the width of the conduits between the surface and various underground reservoirs.

Received 22 April; accepted 7 June 2013.
Published online 31 July 2013.

1. Spencer, J. R. *et al.* in *Saturn from Cassini-Huygens* (eds Dougherty, M. K., Esposito, L. W. & Krimigis, S. M.) 683–724 (Springer, 2009).
2. Dougherty, M. K. *et al.* Identification of a dynamic atmosphere at Enceladus with the Cassini Magnetometer. *Science* **311,** 1406–1409 (2006).
3. Hansen, C. J. *et al.* Enceladus' water vapor plume. *Science* **311,** 1422–1425 (2006).
4. Waite, J. H. *et al.* Cassini Ion and Neutral Mass Spectrometer: Enceladus plume composition and structure. *Science* **311,** 1419–1422 (2006).
5. Porco, C. C. *et al.* Cassini observes the active south pole of Enceladus. *Science* **311,** 1393–1401 (2006).
6. Ingersoll, A. P. & Ewald, S. P. Total particulate mass in Enceladus plumes and mass of Saturn's E ring inferred from Cassini ISS images. *Icarus* **216,** 492–506 (2011).
7. Hedman, M. M. *et al.* Spectral observations of the Enceladus plume with Cassini-VIMS. *Astrophys. J.* **693,** 1749–1762 (2009).
8. Postberg, F. *et al.* The E-ring in the vicinity of Enceladus. *Icarus* **193,** 438–454 (2008).
9. Postberg, F., Schmidt, J., Hillier, J., Kempf, S. & Srama, R. A salt-water reservoir as the source of a compositionally stratified plume on Enceladus. *Nature* **474,** 620–622 (2011).
10. Spencer, J. R. *et al.* Cassini encounters Enceladus: background and the discovery of a south polar hot spot. *Science* **311,** 1401–1405 (2006).
11. Nimmo, F., Spencer, J. R., Pappalardo, R. T. & Mullen, M. E. Shear heating as the origin of the plumes and heat flux on Enceladus. *Nature* **447,** 289–291 (2007).
12. Hurford, T. A., Helfenstein, P., Hoppa, G. V., Greenberg, R. & Bills, B. G. Eruptions arising from tidally controlled periodic openings of rifts on Enceladus. *Nature* **447,** 292–294 (2007).
13. Meyer, J. & Wisdom, J. Tidal heating in Enceladus. *Icarus* **188,** 535–539 (2007).
14. Tobie, G., Cadek, O. & Sotin, C. Solid tidal friction above a liquid water reservoir as the origin of the south pole hotspot on Enceladus. *Icarus* **196,** 642–652 (2008).
15. Smith-Konter, B. & Pappalardo, R. T. Tidally driven stress accumulation and shear failure of Enceladus's tiger stripes. *Icarus* **198,** 435–451 (2008).
16. Hurford, T. A. *et al.* Geological implications of a physical libration on Enceladus. *Icarus* **203,** 541–552 (2009).
17. Saur, J. *et al.* Evidence for temporal variability of Enceladus' gas jets: modeling of Cassini observations. *Geophys. Res. Lett.* **35,** L20105 (2008).
18. Smith, H. T. *et al.* Enceladus plume variability and the neutral gas densities in Saturn's magnetosphere. *J. Geophys. Res.* **115,** A10252 (2010).
19. Hansen, C. J. *et al.* The composition and structure of the Enceladus plume. *Geophys. Res. Lett.* **38,** L11202 (2011).
20. Porco, C. *et al.* Jetting activity and thermal emission across the south polar terrain of Enceladus: observations and comparisons with shear-heating models. *AGU Fall Meet. Abstr.* P13F-02 (2011).
21. Hurford, T. A., Helfenstein, P. & Spitale, J. N. Tidal control of jet eruptions on Enceladus as observed by Cassini ISS between 2005 and 2007. *Icarus* **220,** 896–903 (2012).
22. Brown, R. H. *et al.* The Cassini Visual and Infrared Mapping Spectrometer (VIMS) investigation. *Space Sci. Rev.* **115,** 111–168 (2004).
23. Schmidt, J., Brilliantov, N., Spahn, F. & Kempf, S. Slow dust in Enceladus' plume from condensation and wall collisions in tiger stripe fractures. *Nature* **451,** 685–688 (2008).

Supplementary Information is available in the online version of the paper.

Acknowledgements We acknowledge the support of the VIMS team, the Cassini project and NASA. This work was supported in part by NASA grant NNX12AC29G. The work of C.M.G. on this project was made possible by the Research Experience for Undergraduates programme at Cornell University.

Author Contributions M.M.H., C.M.G. and P.D.N. performed the data analysis. R.N.C., along with P.D.N., C.S., R.H.B., K.H.B. and B.J.B., planned the observations, and provided the data from the VIMS instrument and the appropriate calibration routines. M.R.S. supported the photometric interpretation of these data. All authors discussed these results.

Author Information Reprints and permissions information is available at www.nature.com/reprints. The authors declare no competing financial interests. Readers are welcome to comment on the online version of the paper. Correspondence and requests for materials should be addressed to M.M.H. (mmhedman@astro.cornell.edu).